

000
001
002
003
004
005
006
007
008
009
010
011

Abstract

We propose a novel approach for the matching of partial deformable shapes in 3D. Inspired by recent advances in 2D template matching techniques, our method relies on the concept of deformable diversity similarity(DDIS), extends and adapts it from an image to the 3D shape domain, and leverages the distinct behavior of this framework in different scales to achieve shape correspondences. We evaluate this framework on the SHREC16 partial matching of deformable shapes and show state of the art performance in achieving sparse correspondences.

1. Introduction

Shape correspondence is a fundamental and challenging problem in computer vision and graphics. It has usage in various applications such as transferring texture and animation. Shapes rarely, if ever manifest in only one pose. While rigid transformations between surfaces is a well researched topic with many adequate solutions, a more challenging problem arises when a shape is deformed non-rigidly, a case all too common for people, animals and objects. Moreover, the shape acquisition process almost always lead to partiality of the scanned object. Occlusions arise from different angles of acquisition, which cause an object to occlude itself, or stem from other occluding objects. An additional type of difficulty which might be occur is topological noise, occurring when shapes touch pn another, thus making sensors unable to seperate them. All of these combined give rise to the challenging problem of partial correspondences, where a deformed and incomplete shape, possibly with topological changes, has to be matched with its full version. The goal of this paper is to deal with this challenging problem.

While in a rigid setting the problem can be solved by RANSAC and ICP like approaches[20, 10], extending these to non-rigid case produces mediocre results due to an underlying assumption of small deformations. Early methods specialized for the non-rigid problem focused on minimization of intrinsic metric distortion[6, 28, ?] and regularity of

Anonymous CVPR submission

Paper ID ****

parts[?, 4]. These methods all contain with them a global assumption of isometry which holds only approximately, these tended to break down with it, and are also unable to handle extreme partiality. Another family of method is based on functional correspondence. These methods model correspondences as a linear operator of a known nature between a space of functions on manifolds[15]. These methods, originally designed for the full shape correspondence scenario have achieved state of the art results on various partial matching tasks in the recent years[13, 29, 18], and produce dense correspondence maps, but are not parallelizable, and their reliance on intrinsic metrics makes them invariant to symmetry.

We take a different approach. We take advantage of the fact that while the isometric property tends to break over large distances, it usually holds approximately in limited environments. These also tend to suffer a lot less from boundary effects, especially when concentrated around the extremities of a shape.

We can thus treat the problem of partial correspondences as matching of multiple templates, each smaller then the partial surface centered around shape landmarks.

In addition, since point descriptors are known to be modified by partiality and deformations, instead of using them directly, we follow the approach off[26](**DDIS**) which tackles template matching in 2D and use simple statistical assumptions on the nature of nearest neighbors between small patch descriptors, along with the assumption of small deformations in medium environments to obtain similarity scores between these partial shape templates.

We analyze the behavior of DDIS similarity in different scales and devise a multi scale scheme which leverages the advantages of each scale while masking their shortcomings.

We show that using this approach, we are able to generate a set of sparse correspondences, which are less prone to symmetrical assignment than functional correspondence reliant methods, and are of superior quality on the SHREC16 Partial matching challenge[8]. We then demonstrate how these sparse correspondences can be used as an input to existing functional correspondence algorithms to obtain dense correspondences or a higher quality.

054
055
056
057
058
059
060
061
062
063
064
065
066
067
068
069
070
071
072
073
074
075
076
077
078
079
080
081
082
083
084
085
086
087
088
089
090
091
092
093
094
095
096
097
098
099
100
101
102
103
104
105
106
107

- 108 In summary, our contributions are:
 109
 110 • A non trivial extension of Deformable Diversity from
 111 2 to 3 Dimensions.
 112
 113 • A modified DDIS similarity measure which is more
 114 well suited to handle matching of templates with a dif-
 115 ferent number of points.
 116
 117 • An empirical analysis of DDIS behavior in different
 118 scales, leading to an improved multi-scale framework.
 119
 120 • A novel multi-template approach to partial matching
 121 of deformable shapes which can both produce state of
 122 the art sparse correspondences, and be used as an input
 123 to functional correspondence algorithms, significantly
 124 improving the results obtained by these.

125 The rest of the work is organized as follows: in section
 126 we go over related works in the field of shape analysis.
 127 Section 3 introduces our Deformable Diversity framework
 128 for 3D shape matching. Experiments and results are given
 129 in section 4, and the conclusions are in section 5. **2. What**
 130 **previous work suggested -key ideas and drawbacks**

- 131 3. Our key ideas
- 132 4. Our results
- 133 5. Major contributions
- 134 6. Roadmap

136 **2. Related work**

138 **2.1. Matching Of Surfaces**

140 As a fundamental problem in computer graphics and vi-
 141 sion, an extensive body of work have been done on the
 142 matching of surfaces. A variety of shape descriptors have
 143 been devised for this task which can be roughly divided in to
 144 2 families. Extrinsic ones, such as PFH[21], SHOT[27] and
 145 FPFH[20] which are usually calculated in euclidean space
 146 and are thus sensitive to non rigid deformations, but can dis-
 147 cern between reflections and are also more robust to noise,
 148 topological artifacts and boundary effects.

149 On the other hand intrinsic features such as Heat[7] and
 150 Wave Kernel signatures[3] are invariant under isometric
 151 transformations, but are very sensitive to partiality and are
 152 unable to discern between symmetric parts.

153 These have been commonly used to generate rough cor-
 154 respondences between surfaces and point clouds, but on
 155 their own are noisy and offer little in terms of bijectivity
 156 and continuity of the solution.

157 Recent works, which address the full correspondence
 158 problem[2, 14, 25, 30] manage to cope with distortion by
 159 using smarter optimization objectives, but use the assump-
 160 tion of a bijection between the shapes, and thus cannot han-
 161 dle significant partiality.

162 **2.2. Partial Matching of Deformable shapes**

163 For the rigid setup an adequate solution exists. Iter-
 164 ative Closest Point(ICP)[1] algorithm, preceded by initial
 165 alignment[22] tackle partial matching successfully. Adapt-
 166 ing this to the rigid setup however has proved to have lim-
 167 ited success due to the alignment which is necessary, and
 168 thus is only fit for very small non-rigid deformation.

169 Early non-rigid partial correspondence methods were
 170 aimed at minimizing distortion Early works which were de-
 171 signed with partial matching in mid[4, 5] solved a com-
 172 bined optimization problem over the metric distortion and
 173 the regularity of corresponding parts. Following works
 174 relaxed the regularity requirement by allowing for sparse
 175 correspondence[28] and controlling the sparsity of which
 176 [19]. Other metric distortion based works[23, 24] mini-
 177 mized the distortion metric over the shape extremities by
 178 doing combinatorial search of least distortion matches and
 179 then densify while refining them in the process. In addi-
 180 tion to only supplying sparse correspondences and having a
 181 high computational complexity, relying only on the intrinsic
 182 distortion metric makes these methods fail when boundary
 183 effects plays a significant role.

184 In[16] a bag of words point-wise descriptors on a part in
 185 conjunction with a constraint on area similarity and the reg-
 186 ularity of the boundary length to produce correspondence
 187 less matching parts without point to point correspondences.

188 Another notable family of works are derived from func-
 189 tional correspondences. Introduced at[15] these assume that
 190 correspondences between spaces of functions on a manifold
 191 can be modeled as a linear operators, approximately diagno-
 192 nal given a smart choice of functions, which, given a small
 193 set of known correspondences can be recovered. The orig-
 194 inal paper used the Laplace Beltrami eigenfunctions. Fol-
 195 lowing works employed joint diagonalization of the Lapla-
 196 cian matrices to find an optimal basis, and[17] extended it
 197 to the setting where the order of the functions is unknown,
 198 by solving for permutation of correspondence as well. It
 199 has been shown in [12] that matrix completion can address
 200 non-isometry and mild partiality. A combination with heat
 201 kernels as a distortion metric[29] has been shown to be
 202 able to handle some partiality, given an initialization with
 203 sparse correspondences, but this relies heavily on obtaining
 204 good initial correspondences, and thus application to partial
 205 matching has only been shown as a proof of concept.

206 Recently [18] had proven that partiality induces a slanted
 207 diagonal structure in the correspondence matrix and found
 208 the Laplacian eigenfunctions from each basis which induces
 209 this structure. Current state of the art[13] uses this notion
 210 in conjunction with joint diagonalization. The main draw-
 211 back of this method, shared with other intrinsic methods, is
 212 its invariance to symmetries. In addition, using sequential
 213 optimization, the entire family of methods cannot be paral-
 214 lelized.

216 **3D Shape Descriptors** 270
217218 **2.3. Template matching in 2D** 271
219220 Template matching in 2D is a well researched topic.
221 Similarly to 3D objects are going complex deformations of
222 pose, and are only seen partially depending on the camera
223 point of view. Recently a series of works which use a very
224 simplistic framework based on the statistical properties of
225 nearest neighbors in low level feature space had made good
226 strides in tackling this complex task.227 **Best Buddies Similarity** Great strides had been
228 achieved in the field of 2D template matching. Best Buddies
229 Similarity[9] is a simple framework which employs a statis-
230 tical assumption in which between two windows containing
231 the same template \mathcal{N}, \mathcal{M} patches maintain Bi Directional
232 Similarity. That is - given a point $n_i \in \mathcal{N}$ and a correspond-
233 ing point $m_j \in \mathcal{M}$ they should maintain a relationship of
234 Bi-Directional Similarity - that is if $NN_{\mathcal{M}}(n_i) = m_j$ then
235 on a matching template we should expect $NN_{\mathcal{N}}(m_j) = n_i$.
236 This led to a significant improvement in template matching.237 **Deformable Diversity Similarity** Building upon the
238 above work, [26] added two additional and rather simple
239 assumptions. The first of which is that the diversity of Near-
240 est Neighbors between corresponding templates should be
241 high. This is actually a prerequisite to a high best buddies
242 similarity score and serves as a rough approximations. For
243 this end diversity is formally defined as:

244
$$DIS = c \cdot |\{n_i \in \mathcal{N} : \exists m_j \in \mathcal{M}, NN(m_j, \mathcal{N}) = n_i\}| \quad (1)$$
 245
246

247 where $|\cdot|$ denotes group size and $c = 1/\min(|\mathcal{M}|, |\mathcal{N}|)$ is
248 a normalization factor. Between non corresponding win-
249 dows, indeed one should expect most points to have no real
250 corresponding point, and thus be mapped to a very and re-
251 mote nearest neighbors. On the other hand, regions contain-
252 ing matching objects are drawn from the same distribution,
253 thus the diversity of nearest neighbors should be high. To
254 accommodate this assumption not only did they rewarded
255 high diversity of nearest neighbors, but also penalized map-
256 ping to the same patch. To this end, another, a negative
257 diversity measure had been defined:

258
$$\kappa(n_i) = |\{m \in \mathcal{M} : NN^a(m, \mathcal{N}) = n_i\}| \quad (2)$$
 259
260

261 With x_i^a denoting the appearance descriptor of point x_i .
262 Thus the contribution of being a nearest neighbor to a patch
263 with multiple nearest neighbors would become $\exp(1 -$
264 $\kappa(NN^a(m_j, \mathcal{N}))$). A final observation made has been that
265 while non rigid deformations do occur, they should be re-
266 stricted, small, in real objects. With the distance on the
267 window pixel grid between 2 nearest neighbor points de-
268 fined as $r_j = d(m_j^l, n_i^l)$ with x_i^l denoting the location of x_i
269 relative to the center of the template, the final Deformable270 Diversity Similarity formulation becomes:
271

272
$$DDIS = c \sum_{\mathcal{M} \leftarrow \mathcal{N}} \frac{1}{1 + r_j} \cdot \exp(1 - \kappa(NN^a(m_j, \mathcal{N}))) \quad (3)$$
 273
274

275 **3. Deformable Diversity for Partial matching
276 of 3D surfaces** 277
277278 **1. Goal of this section** In this section we will describe
279 the Deformable Diversity framework for matching of de-
280 formable shapes, as we had adjusted it for the 3D setting.
281 The algorithm follows the ideas presented by [26], and ad-
282 justs them for the unique challenges posed by the 3D setting
283 in which information is sparser and of varying density, and
284 the scenario of partial shape correspondence in which the
285 part and the scene are of comparable area.286 **2. Key ideas of the algorithm** As stated above, a lot of
287 the key ideas are similar to the 2D scenario - the feature
288 nearest neighbor field between a part and his transformed
289 version tends to give rise to a high diversity of matches. In
290 addition, correct corresponding points between a template
291 and a matching object should lie in nearby regions with
292 relation to some reference point on the template. We im-
293 prove upon these with the realization that while deforma-
294 tion should hold very roughly for the entire part, it tends to
295 hold better the closer we are to the reference point. This
296 gives rise to a framework in which instead of matching the
297 whole template at once, we break it into multiple tasks of
298 smaller template matching, effectively using DDIS as a mid
299 level psuedo-metric to describe part similarity. Finally we
300 employ a strategy of choosing extremities on the surface for
301 the central points of the mini templates. Picking these ex-
302 tremities together with the matching of mini templates tends
303 to both mitigate boundary effects, and pushes the size of the
304 object in the full shape and the partial shape to be more sim-
305 ilar. Finally, we observe that DDIS has different properties
306 at different scales and thus employ a multi-scale cascade to
307 take advantage of this fact.308 **3. Overview of the algorithm (Preprocessing (normal es-
309 timation, FPFH), Finding the landmark points, computing
310 DDIS correspondence for pairs, computing correspondence
311 of surfaces) Include an image of this general overview.**312 The outline of the algorithm is as follows: we first cal-
313 culate the nearest neighbor field between the full shape and
314 the part - we begin by calculating local point descriptors
315 and use ANN to find for each point $m_i \in \mathcal{M}$ its most similar
316 point $NN^S(m_i, \mathcal{N})$. We then use an extremity locating al-
317 gorithm to find suitable mini template centers. for each of
318 those we extract a surface piece of a certain geodesic radius
319 around it to serve as the mini template. Then for each of
320 these templates we look for the most similar piece of surface
321 of a similar radius around each point on \mathcal{M} . We use DDIS
322 as a similarity measure between all pairs of mini templates.
323 The points whose surface patch maximize this function for

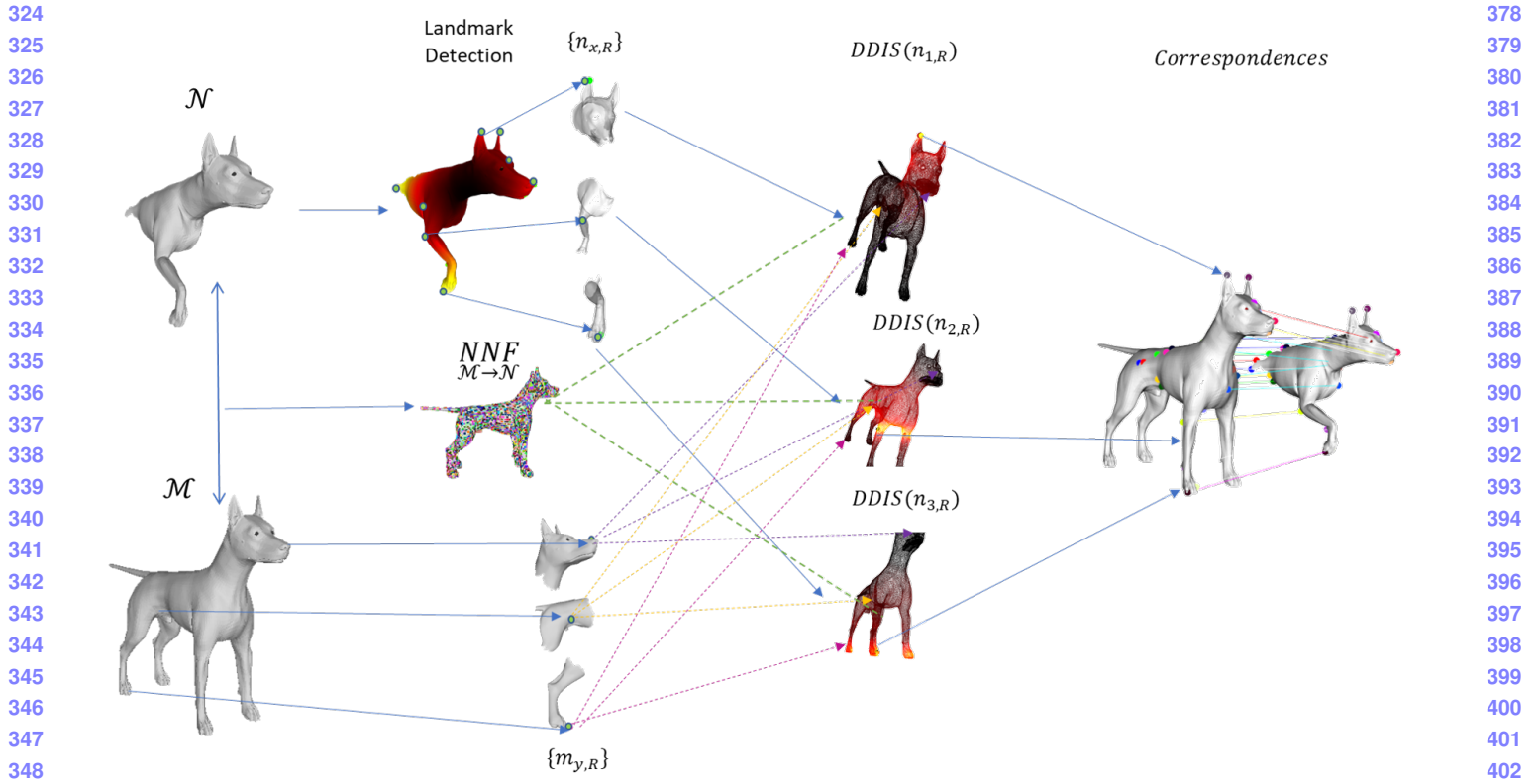


Figure 1. High level illustration of the DDIS Partial Correspondence pipe.

each mini template are then set as the corresponding points to their centers.

4. Road-map to the section We will begin with a description of the changes made for the deformable diversity framework as a result of moving from 2D to 3D. We will then go over the specific stages of preprocessing necessary for Deformable Diversity in 3D. We will continue with describing the matching process of a single mini template on a full shape. Finally we will describe the extraction of multiple correspondences using this framework.

3D Deformable Diversity Formulation

The nature of 3D data gives rise to unique problems which do not occur in the 2D scenario. Data is distributed in space both sparsely and with varying densities - the amount of data points occupying a given volume can vary drastically.

A second problem arises from the absence of a regular grid. These problems require different definitions for key components to the 2D deformable diversity formulation. For this work we chose the image patch to be replaced by a neighborhood which is required to calculate a selected shape descriptor, usually a small sphere in euclidean space or a surface patch in a small environment with a radius r_F . The search window of a template is replaced by a bigger environment around a chosen point, one which encompasses the entire desired part ,with a radius denoted by R . The

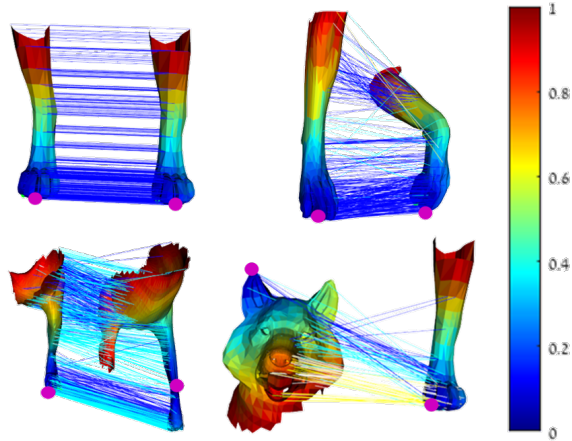


Figure 2. Illustration of Diversity Similarity between different shapes. Geodesic Distances are color coded by the jet scheme. You can notice that on identical pieces, and even on deformed matching pieces there are multiple diverse matches, most of which are colored in blue to indicate very similar distances from the source point, whereas on different pieces most lines map to very few points and a lot of yellow lines (high deformation) exist

pixel grid distance is replaced by either a euclidean distance $d_{Euc}(x^l, y^l)$ (in the case of point cloud) or geodesic distance

432 $d_{Geo}(x^l, y^l)$ (for surface meshes). Given these DDIS between shape parts $\mathcal{M}_{x,R}$ and $\mathcal{N}_{y,R}$ can be naively formulated as:

$$436 \quad DDIS = c \cdot \sum_{m_j \in \mathcal{M}_{x,R}} \frac{\exp(1 - \kappa(NN^S(m_j, \mathcal{N}_{y,R})))}{1 + r_j} \quad (4)$$

439 where $\mathcal{M}_{x,R}$ and $\mathcal{N}_{y,R}$ are the shape parts in a radius R surrounding the points m_x and n_y respectively, and $r_j = |d(m_j^l, m_x^l) - d(NN^S(m_j, \mathcal{N}_{y,R})^l, n_y^l)| / (\gamma \cdot R)$, where γ is a tunable parameter and $c = 1/\min|\mathcal{N}_{y,R}|, |\mathcal{M}_{x,R}|$.

443 However, we wouldn't like to penalize our similarity score in case of repeating patterns or symmetrical shapes which have both symmetries in the template search window. Intuitively and empirically the exponent is too harsh and indeed unnecessary as both deformity and diversity will attenuate the score in case of multiple nearest neighbors. On the other hand, we wouldn't want to reward far correspondences at all. **explain why – can we see it visually on the same example? no visual example yet, as the partition into smaller templates mitigates some of the problems of the old formulation it seems, though the new one has still given an extra 2 percent of accurate matches even in the mini template setting** To account for this the following formulation has been found to work better: given a point $n_i \in \mathcal{N}_{y,R}$ has a set of points $\mathcal{M}_{n_i} = \{m_j \in \mathcal{M}_{j,R} : NN^S(m_j, N_{y,R}) = n_i\}$ for which it is the nearest neighbor, we define $m'_i = \operatorname{argmin}_{m_j \in \mathcal{M}_{n_i}}(r_j)$ and r'_i the minimal distortion distance our corrected formula becomes

$$462 \quad DDIS(\mathcal{N}_{y,R}, \mathcal{M}_{x,R}, \gamma) = \sum_{m'_i} \frac{1}{1 + r'_i} \quad (5)$$

465 This equation still promotes both diversity and low deformations, but is less biased towards unsymmetrical surfaces.

468 Algorithm 1 3DIS Correspondence

```
469 procedure DDIS MATCH( $\mathcal{M}, n_y, \mathcal{N}, R_{thresh}, NNF$ ) $\triangleright$   

470   Returns the location of the  $n_i \in \mathcal{N}$  in  $\mathcal{M}$   

471    $\mathcal{N}_{y,R} \leftarrow \{N_i \in \mathcal{N} : d_{Geo}(n_i, n_x) < R_{thresh}\}$   

472    $Similarity_{max} \leftarrow 0$   

473   for  $m_x \in \mathcal{M}$  do  $\triangleright$  DDIS calculation Loop  

474      $\mathcal{M}_{x,R} \leftarrow \{m_j \in \mathcal{M} : d_{Geo}(m_x, m_j) < 1.05 \cdot R_{thresh}\}$   

475      $Similarity[x] \leftarrow DDIS(\mathcal{M}_{x,R}, \mathcal{N}_{y,R})$   

476     if  $Similarity[x] > Similarity_{max}$  then  

477        $Similarity_{max} \leftarrow Similarity[x]$   

478        $m_y^* \leftarrow m_x$   

479     end if  

480   end for  

481   return  $m_y^*$   

482 end procedure
```

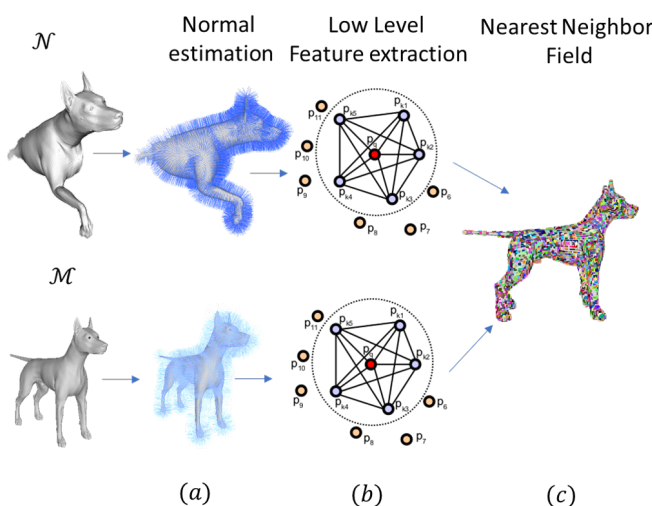


Figure 3. Nearest Neighbor Field calculation.

3.1. DDIS Template Matching

Goal of the algorithm In this section we go over the flow of template matching of 3D shapes using DDIS, the solution of which constitutes the core of our partial shape matching. Given a template $\mathcal{N}_{y,R}$ with a reference point n_y as its center and a maximal distance R , we aim to find on and object \mathcal{M} which has a deformed version of it, the corresponding surface piece $\mathcal{M}_{y*,R}$ and its center m_y^* . The solution is obtained by finding the point on \mathcal{M} whose surrounding surface maximizes the above mentioned DDIS measure. **key ideas**

Overview We'll first give an overview, and then give an extended description of each of each stage.

We start by calculating the normals for \mathcal{M} and \mathcal{N} . We than calculate local patch descriptors for each patch of some neighborhood around the points in each mesh(For our purpose FPFH seemed to work the best of our tested descriptors). Having calculated these descriptors we calculate a nearest neighbor field by finding for each patch in \mathcal{M} it's Nearest Neighbor in \mathcal{N} . We now find the distance of every point $n \in \mathcal{N}$ to the desired point n_y for a desired neighborhood R . We now go over every point $m_x \in \mathcal{M}$. For each we extract the surface $\mathcal{M}_{x,R}$ in an R neighborhood around it. We take notice that while the above stages are done here in the context of template matching for one template, when matching multiple templates all of the above calculations have to be done only once between the shapes, with the exception of geodesic distance field extraction for the template itself.

Now we calculate our DDIS similarity measure of this surface with $\mathcal{N}_{x,R}$ which has n_y as it's center. Having done that for every location, the point m_y^* which gets the maximal DDIS Score is deemed the corresponding point to n_y .

Point Normal Estimation There are various schemes

540 for the estimation of point normals given a triangulated
 541 mesh surface. We have picked the one which is available in
 542 the standard PCL. Given a vertex p_i on a triangulated mesh
 543 \mathcal{X} and it's associated polygons $\{A_j\}_{j=1}^k$ and their normals
 544 N_{A_j} the point normal $N_i = \sum_{j=1}^k |A_j| \cdot N_{A_j}$

545 **Local Patch Size choice** DDIS as defined by [] uses
 546 patch descriptors as low level features for their similarity
 547 measure. While a patch in an image can be defined by
 548 the images grid no such grid exists on 3D point clouds and
 549 meshes, where density of data points can vary. Thus a patch
 550 has to be defined by some geometric measure. While the
 551 more robust way to define it would be using geodesic distance,
 552 since we are talking a small environment around a
 553 point on the mesh we have found that for practical purposes
 554 a patch in a defined euclidean radius around a point serves
 555 well enough. We pick this radius in the following way:
 556 given the full surface mesh \mathcal{M} we define a characteristic
 557 length $D_{\mathcal{M}} = \sqrt{\text{Area}(\mathcal{M})}$, and tune a parameter α to obtain
 558 $r_F = \frac{\alpha}{100} * D_{\mathcal{M}}$

559 **Local Patch Descriptor** A lot of local shape descriptors
 560 have been used successfully in 3D shape analysis.
 561 We have tested the following descriptors which are included
 562 in the Point Cloud Library: ROPS[?, Theorem
 563 2] PFH[] SHOT[], HKS[], SIHKS[], ROPS[] and FPFH[].
 564 Out of these 4 FPFH has achieved the best performance,
 565 and thus the descriptor for the local patch has been chosen
 566 to be FPFH. **Nearest Neighbor Field** As an intermediate
 567 stage towards the calculation of Deformable Diversity
 568 Similarity measure, the calculation of the nearest neighbor
 569 field(will be abbreviated as NNF) needs to be calculated.
 570 Thus for every patch $m \in \mathcal{M}$ we have to find the patch
 571 on the template $n \in \mathcal{N}$ which resembles it the most.
 572 For $FPFH$, $NN^S(m_j, \mathcal{N})$ is defined
 573 $NN^S(m_j, \mathcal{N}) \equiv \underset{i}{\operatorname{argmin}} \chi^2(FPFH(m_j], FPFH(n_i))$
 574 and the Nearest Neighbor Field is the set of all these
 575 correspondences.

576 **DDIS calculation** For every point in $m_x \in \mathcal{M}$ we then
 577 extract a surface part $\mathcal{M}_{x,R}$ with a radius R around it and
 578 calculate deformable diversity around it. The point which
 579 maximizes DDIS gives us a correspondence (n_y, m_y*) .
 580 Since as we will show in the results section, imperfections
 581 in the isometry assumption lead to considerable localization
 582 errors, we move to a multiple template matching framework
 583 using DDIS, as will be described in the next section.

584 3.2. DDIS Sparse Correspondences

585 A key takeaway from experimenting with DDIS as a
 586 template matching algorithm for partial matching has been
 587 that isometry does not hold, at least not globally. It does
 588 however, hold pretty well locally, especially at extremities.
 589 To this end we devise multiple template framework for
 590 Partial correspondences of deformable shape. We first obtain

591 the landmarks $F = \{f\}_i$ as described in []. We then choose
 592 a partiality radius $R = \gamma \cdot R$ and extract surface parts $\mathcal{N}_{i,R}$
 593 around each extremity point. Finally for each point we calculate
 594 DDIS to get it's correspondence.

595 **Landmark Extraction** We follow the work of [Sagi
 596 Katz Ayellet Tal] to obtain interesting landmark points.
 597 Given a shape the work employs the following framework
 598 to extract it's extremities. A point is detected as an extremity
 599 if it fulfills 2 conditions: - it's sum of geodesic distances
 600 is a local extrema, formally, for $v \in S$, where S is a surface
 601 mesh, we define the set of points with a direct edge to it as
 602 N_v , the point is a critical point if :

$$\sum_{v_i \in S} d_{geo}(v, v_i) > \sum_{v_i \in S} d_{geo}(v_n, v_i), \forall v_n \in N_v \quad (6)$$

603 An additional requirement for it to be an extremities is for
 604 it to lie on the convex hull of the shape's MDS. In this work
 605 we have dropped the last condition, but chose N_v* - a neighbor-
 606 hood of $0.03 \cdot \sqrt{\text{Area}(S)}$.

607 Algorithm 2 3DIS Sparse Correspondences

```

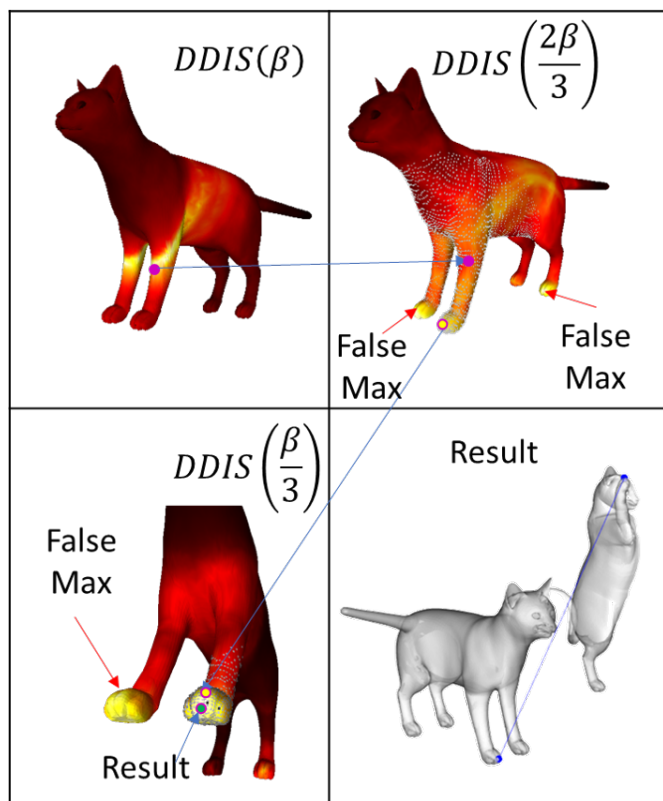
608 procedure DDIS CORRESPONDENCE( $\mathcal{M}, \mathcal{N}, \alpha, \beta, \gamma$ ) ▷
609   Returns point correspondence for critical points on  $\mathcal{N}$ 
610    $r_F \leftarrow \alpha/100 \cdot \sqrt{\text{Area}(\mathcal{M})}$ 
611    $R_{thresh} \leftarrow \beta/100 \cdot \sqrt{\text{Area}(\mathcal{M})}$ 
612    $N_{\mathcal{M}} \leftarrow \text{ComputeNormals}(\mathcal{M})$ 
613    $N_{\mathcal{N}} \leftarrow \text{ComputeNormals}(\mathcal{N})$ 
614    $F_{\mathcal{M}} \leftarrow FPFH(\mathcal{M}, N_{\mathcal{M}}, r_F)$ 
615    $F_{\mathcal{N}} \leftarrow FPFH(\mathcal{N}, N_{\mathcal{N}}, r_F)$ 
616    $NNF_{\mathcal{M} \rightarrow \mathcal{N}} \leftarrow ANN(F_{\mathcal{M}}, F_{\mathcal{N}})$ 
617    $\mathcal{N}_c = \{n : \sum_{n_i \in \mathcal{N}} d_{geo}(n, n_i) > \sum_{n_i \in \mathcal{N}} d_{geo}(n_N, n_i), \forall n_N : d_{geo}(n, n_N) < 0.03 \cdot \sqrt{\text{Area}(\mathcal{M})}\}$ 
618   for  $n_y \in \mathcal{N}_c$  do ▷ DDIS calculation Loop
619      $m_{c*} \leftarrow DDIS\_Correspondence(\mathcal{M}, n_y, \mathcal{N}, \alpha, \beta, \gamma)$ 
620   end for
621   return  $\mathcal{M}_c \times \mathcal{N}_c = \{m_{c*}, n_c\}$ 
622 end procedure
623
624
625
626
627
628
629
630
631
632
633
634
635
636
637
638
639
640
641
642
643
644
645
646
647
```

648 **Landmark Template Matching** For this end, we create
 649 a template for each landmark point - we collect all surface
 650 point in a geodesic neighborhood around it of $\beta \cdot \sqrt{\text{area}(\mathcal{M})}$
 651 where for this case a good β (0.2, 0.5) where larger beta
 652 prevents global scale error, such as a cats paw being mapped
 653 to a hind paw, while smaller beta promotes tighter localiza-
 654 tion on the part itself. This can be seen in Figure[] While it
 655 might seem natural to calculate a different nearest neighbor
 656 field for each landmark template it has been empirically
 657 found that using the global nearest neighbor field gives
 658 much better results. This is probably due to the fact that the
 659 nearest neighbor field encodes global information when ob-
 660 tained this way and eliminates local distractors. Each land-

648 mark template is compared to all surface parts of a similar
 649 R on \mathcal{M} to obtain final point correspondences.
 650

651 652 3.3. Cascaded Multi-Scale DDIS

653 The observation of the effects of the choice of β and the
 654 trade-off between finer localization and avoidance of global
 655 errors naturally leads to the adoption of a multi scale frame-
 656 work. We calculate *DDIS* score for multiple *beta* values,
 657 and use the location obtained with a large beta to select a
 658 narrow environment in which we look for the maximum
 659 of *DDIS* with a smaller value *beta*, thus using the larger
 660 scale to get a rough global location, and the smaller scale
 661 to fit it into a more exact location. While this might be
 662 done at multiple custom scales we have found that the triplet
 663 $\beta, 2 \cdot \beta/3, \beta/3$ works well.
 664



691 Figure 4. Illustration of the multi scale framework. Gray point are
 692 the area chosen by the previous scale to be valid. It can be seen
 693 that Wrong maxima in lower scales are ignored due to this process
 694

695 696 697 4. Experiments and results

698 In this section we will briefly go over the experiments
 699 performed and their results. We'll introduce the datasets,
 700 detail our experiments and their results
 701

702 4.1. Datasets

703 In this section we will briefly go over the available
 704 Datasets
 705

706 4.1.1 SHREC 2016

707 The SHREC partial matching dataset consists of 8 base,
 708 neutral pose models: cat, centaur, dog, horse, wolf, and 3
 709 humans – 2 males, and 1 female. Each basic model has
 710 corresponding deformed partial shapes obtained either by
 711 cutting the shape with a plane or by adding holes on a de-
 712 formed shape. The set has been divided into train and test
 713 sets. The train set is composed of 15 cuts for each base
 714 models totaling 120 models, and 10 holed shpaes for each
 715 model for which ground truth point to polygon correspon-
 716 dences has been provided in barycentric coordinates. The
 717 test set is composed of additional 200 cuts and 200 holed
 718 shapes.
 719

720 4.2. Error Metrics

721 The output of partial matching algorithms (as defined
 722 in[8]) are sub-vertex point-to-point correspondences be-
 723 tween partial shapes. For all experiments we use the stan-
 724 dard practice of not penalizing symmetric solutions. Qual-
 725 ity is measured according to the Princeton benchmark pro-
 726 tocol [11]. For a pair of points $(x, y) \in \mathcal{N} \times \mathcal{M}$ between
 727 the full object \mathcal{M} and the partial shape \mathcal{N} produced by an
 728 algorithm, where (x, y^*) is the ground truth correspondence
 729 the inaccuracy is measured by
 730

$$\varepsilon(x) = \frac{d_{\mathcal{M}}(y, y^*)}{\sqrt{\text{area}(\mathcal{M})}} \quad (7)$$

731 where $d_{\mathcal{M}}(y, y^*)$ is the geodesic distance on \mathcal{M} , and has
 732 units of normalized length on \mathcal{M} . For dense correspon-
 733 dences over a dataset, $\varepsilon(x)$ is averaged over all matching
 734 instances.
 735

736 4.2.1 Central Points Localization

737 In this experiment we have chosen for each Template mesh
 738 the center point c_T and tried to match it to a point on the ob-
 739 ject using DDIS. Experiments have been done using FPFH,
 740 PFH and SHOT as patch descriptors with patch radiiuses of
 741 [2, 3, 4, 5], the results of the opimal parameter for each
 742 descriptor are illustrated in fig. and visualizations of simi-
 743 larity maps of cuts are provided in fig. . It can be seen that
 744 good localization is obtained for points on a smooth sur-
 745 face, under high partiality conditions and strong deforma-
 746 tions. Bad matches occur when a matched point resides on
 747 a heavily deformed patch, and when salient anchor points
 748 are deformed or cut. Analysis of these results shows a drift
 749 in localization occurs when salient features are divided by
 750

756

757

758

759

760

761

762

763

764

765

766

767

768

769

770

771

772

773

774

775

776

777

778

779

780

781

782

783

784

785

786

787

788

789

790

791

792

793

794

795

796

797

798

799

800

801

802

803

804

805

806

807

808

809

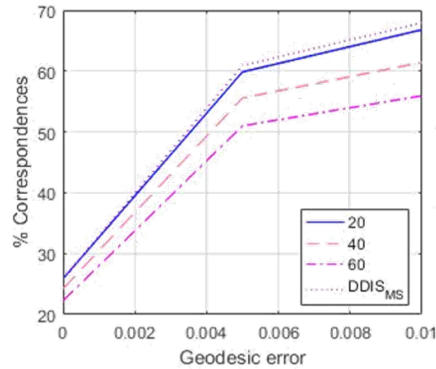


Figure 5. Effect of the β parameter on the results: it can be seen that a smaller beta promotes better localization in a small neighborhood, while higher values of β lead to more local errors but are more robust to global errors. It can be seen that the multi-scale cascade achieves better results both locally and globally.

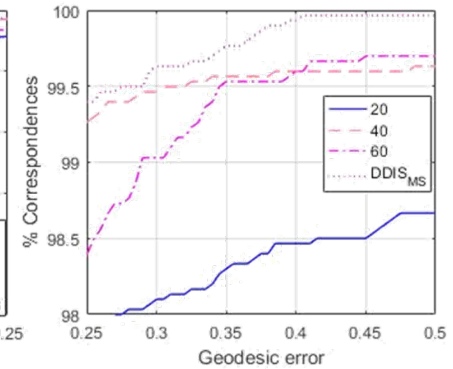
strong unisometric deformations which serve as the motivation for the multiple template matching framework.

4.3. Sparse Correspondences on the SHREC16 Test set

In this experiment we have tested the performance of DDIS in producing sparse correspondences on the SHREC16 Partial Matching of Deformable Shapes competition. We had tuned our parameters on the SHREC16 training dataset using only the cuts part of it. The best results had been produced using FPFH with $r_F = 0.04\sqrt{\text{Area}(\mathcal{M})}$, and a piece size radius $R_{thresh} = 0.3\sqrt{\text{Area}(\mathcal{M})}$. For Geodesic distances we have found the fast marching algorithm to work the fastest, while giving the lowest error w.r.t. to exact geodesics. For a 10,000 vertices mesh it takes 60s to produce a full distance matrix, Though it should be noted this algorithm has a more efficient GPU implementation. FPFH and Nearest Neighbor field takes 2 s' and similarity between 2 pieces of 10000 vertices each takes 25s on average, running on a single thread of i7-2700k. Unlike optimization based algorithms this is highly parallelizable. We achieve results comparable to the state of the art [13] quality wise, even though sparser in nature on both the Cuts and the Holes datasets, Where a particularly impressive result is reported on the Holes dataset. A further look reveals even more reliable results can be obtained taking only the extremity points not lying on the mesh longest boundary, but they will be more sparse

	PFM	RF	IM	EN	GT	DIS	DIStoBound
cuts	dense	dense	61.3	87.8	51.0	27.9	14.5
holes	dense	dense	78.2	112.6	76.4	77.3	52.11

Table 1. mean number of correspondence obtained by the algorithms in the SHREC 16 competitor and our algorithm



References

- [1] D. Aiger, N. J. Mitra, and D. Cohen-Or. 4pointss congruent sets for robust pairwise surface registration. *ACM Trans. Graph.*, 27(3):85:1–85:10, Aug. 2008. 2
- [2] N. Aigerman, R. Poranne, and Y. Lipman. Seamless surface mappings. *ACM Transactions on Graphics (TOG)*, 34(4):72, 2015. 2
- [3] M. Aubry, U. Schlickewei, and D. Cremers. The wave kernel signature: A quantum mechanical approach to shape analysis. In *Computer Vision Workshops (ICCV Workshops), 2011 IEEE International Conference on*, pages 1626–1633. IEEE, 2011. 2
- [4] A. M. Bronstein and M. M. Bronstein. Not only size matters: regularized partial matching of nonrigid shapes. In *Computer Vision and Pattern Recognition Workshops, 2008. CVPRW’08. IEEE Computer Society Conference on*, pages 1–6. IEEE, 2008. 1, 2
- [5] A. M. Bronstein, M. M. Bronstein, A. M. Bruckstein, and R. Kimmel. Partial similarity of objects, or how to compare a centaur to a horse. *International Journal of Computer Vision*, 84(2):163, 2009. 2
- [6] A. M. Bronstein, M. M. Bronstein, and R. Kimmel. Generalized multidimensional scaling: a framework for isometry-invariant partial surface matching. *Proceedings of the National Academy of Sciences*, 103(5):1168–1172, 2006. 1
- [7] M. M. Bronstein and I. Kokkinos. Scale-invariant heat kernel signatures for non-rigid shape recognition. In *Computer Vision and Pattern Recognition (CVPR), 2010 IEEE Conference on*, pages 1704–1711. IEEE, 2010. 2
- [8] L. Cosmo, E. Rodolà, M. Bronstein, A. Torsello, D. Cremers, and Y. Sahillioglu. Shrec’16: Partial matching of deformable shapes. *Proc. 3DOR*, 2, 2016. 1, 7
- [9] T. Dekel, S. Oron, M. Rubinstein, S. Avidan, and W. T. Freeman. Best-buddies similarity for robust template matching. In *Proceedings of the IEEE Conference on Computer Vision and Pattern Recognition*, pages 2021–2029, 2015. 3
- [10] D. Holz, A. E. Ichim, F. Tombari, R. B. Rusu, and S. Behnke. Registration with the point cloud library: A modular frame-

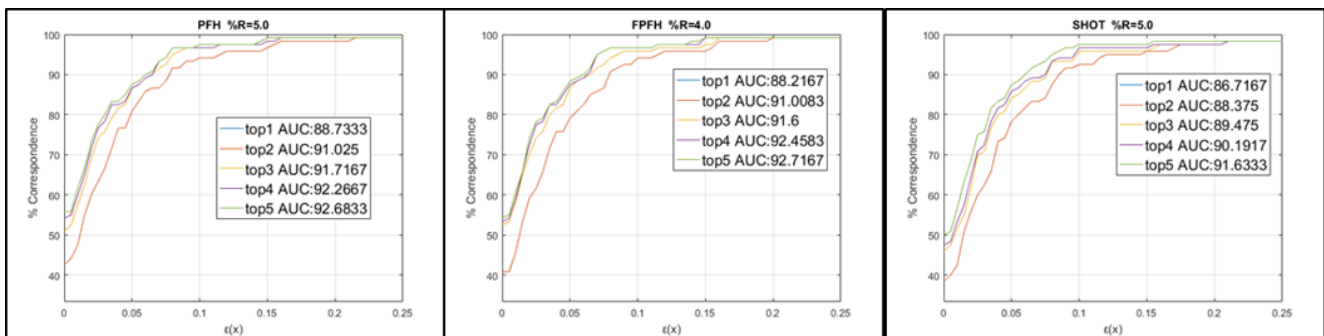
864
865
866
867
868
869
870
871
872
873
874

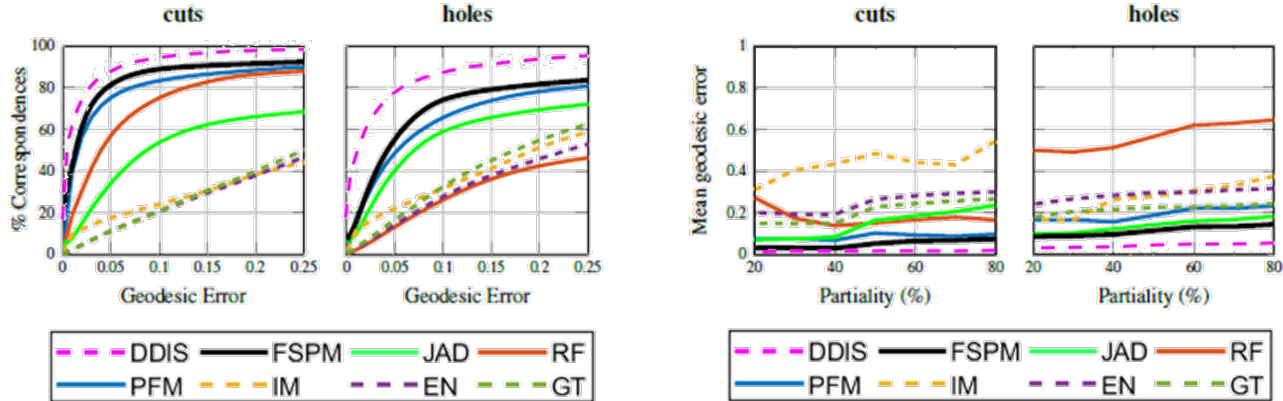
Figure 6. Comparison between descriptors: we show curves for the minimal distance of the top results. a noticeable addition occurs when adding the 2nd best match

877

878
879

With Boundary Points

880

881
882
883
884
885
886
887
888
889
890
891
892
893
894
895
896
897
898
899
900
901
902
903
904
905
906
907
908
909

Discarding Boundary Points

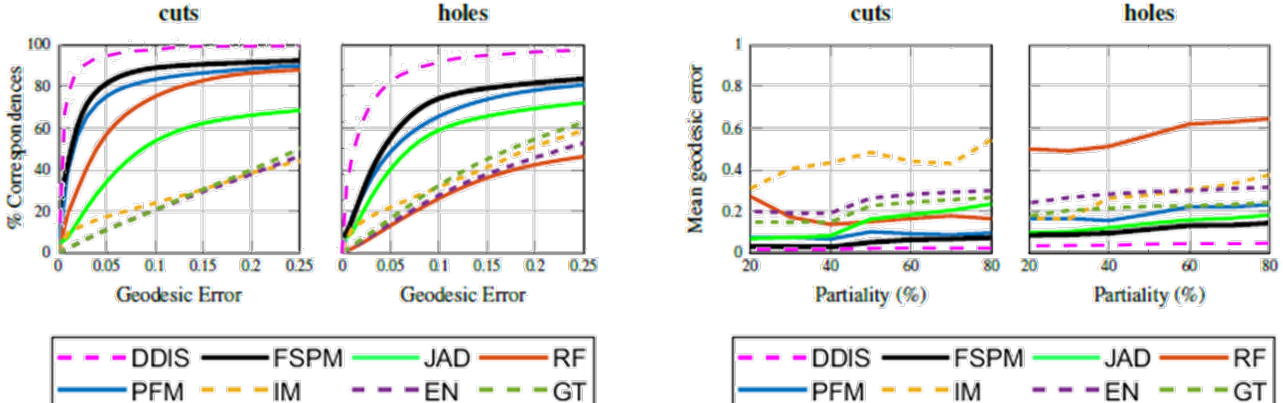


Figure 7. comparison with other state of the art algorithms - it can be seen that although sparse in nature, the correspondence obtained by DDIS are much more accurate than the other methods. A separate analysis has been done for correspondences which include boundary points, which tend to be more noisy, and internal points which are more sparse

913

914 work for aligning in 3-d. *IEEE Robotics & Automation Magazine*, 22(4):110–124, 2015. 1

[11] V. G. Kim, Y. Lipman, and T. Funkhouser. Blended intrinsic maps. In *ACM Transactions on Graphics (TOG)*, volume 30,

- page 79. ACM, 2011. 7
- [12] A. Kovnatsky, M. M. Bronstein, X. Bresson, and P. Vandergheynst. Functional correspondence by matrix completion. In *Proceedings of the IEEE conference on computer*

918
919
920
921
922
923
924
925
926
927
928
929
930
931
932
933
934
935
936
937
938
939
940
941
942
943
944
945
946
947
948
949
950
951
952
953
954
955
956
957
958
959
960
961
962
963
964
965
966
967
968
969
970
971

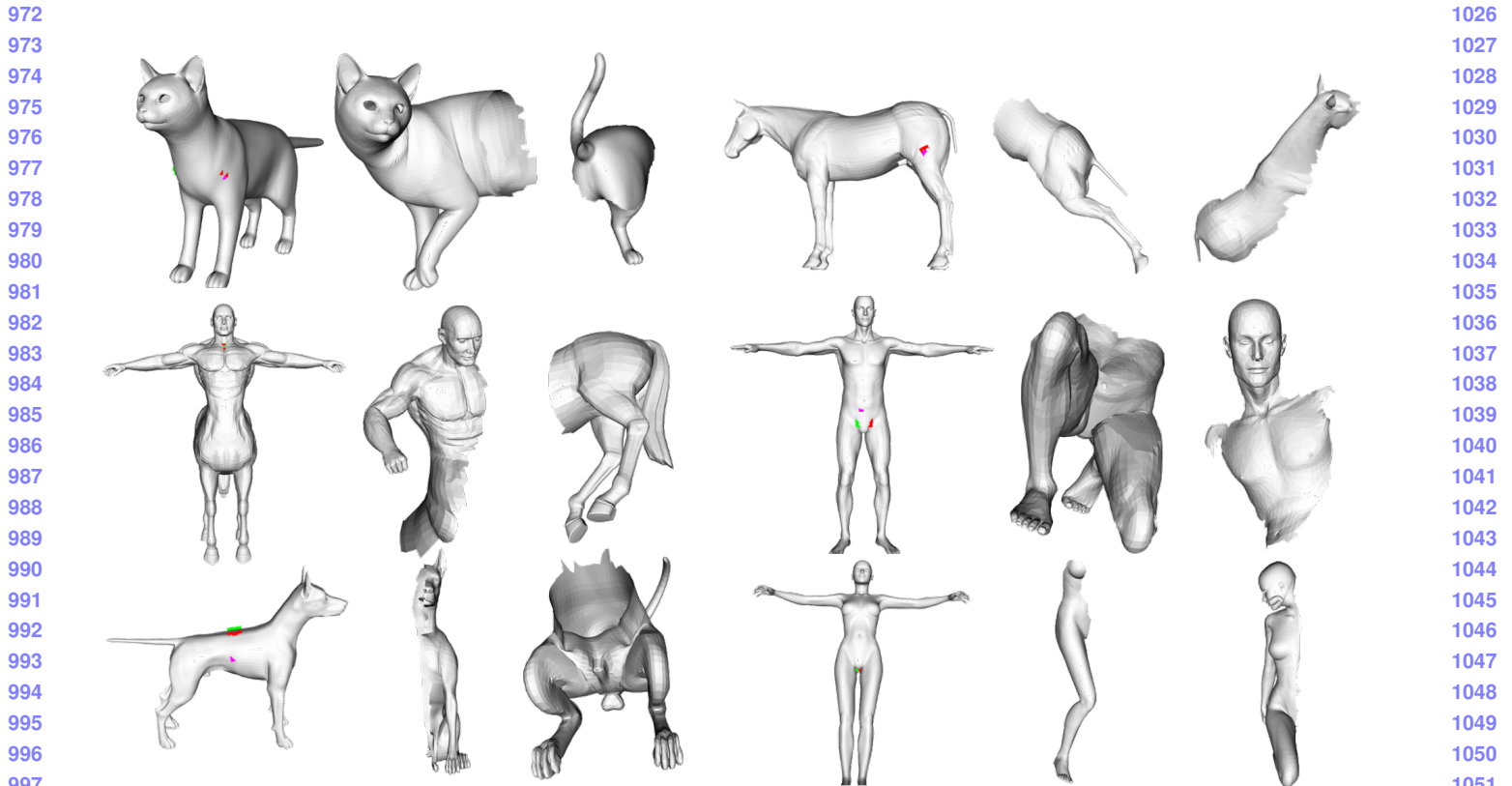


Figure 8. SHREC 16 cuts partial matching dataset.

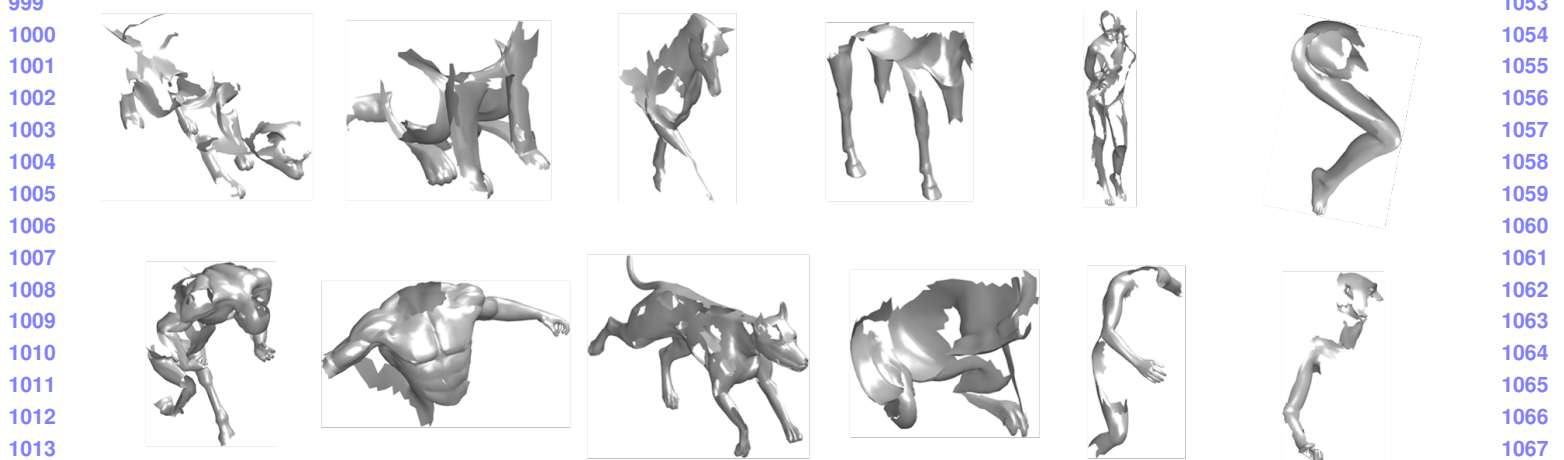


Figure 9. SHREC 16 holes partial matching dataset.

vision and pattern recognition, pages 905–914, 2015. 2

- 1018 [13] O. Litany, E. Rodolà, A. M. Bronstein, and M. M. Bronstein.
1019 Fully spectral partial shape matching. In *Computer Graphics
1020 Forum*, volume 36, pages 247–258. Wiley Online Library,
1021 2017. 1, 2, 8
- 1022 [14] H. Maron, N. Dym, I. Kezurer, S. Kovalsky, and Y. Lip-
1023 man. Point registration via efficient convex relaxation. *ACM
1024 Transactions on Graphics (TOG)*, 35(4):73, 2016. 2
- 1025 [15] M. Ovsjanikov, M. Ben-Chen, J. Solomon, A. Butscher, and

L. Guibas. Functional maps: A flexible representation of
maps between shapes. *ACM Trans. Graph.*, 31(4):30:1–
30:11, July 2012. 1, 2

- [16] J. Pokrass, A. M. Bronstein, and M. M. Bronstein. Partial
shape matching without point-wise correspondence. *Nu-
merical Mathematics: Theory, Methods and Applications*,
6(1):223–244, 2013. 2
- [17] J. Pokrass, A. M. Bronstein, M. M. Bronstein, P. Sprech-
mann, and G. Sapiro. Sparse modeling of intrinsic cor-

- 1080 respondences. In *Computer Graphics Forum*, volume 32,
 1081 pages 459–468. Wiley Online Library, 2013. 2
- 1082 [18] E. Rodolà, L. Cosmo, M. M. Bronstein, A. Torsello, and
 1083 D. Cremers. Partial functional correspondence. In *Computer*
 1084 *Graphics Forum*, volume 36, pages 222–236. Wiley Online
 1085 Library, 2017. 1, 2
- 1086 [19] E. Rodola, A. Torsello, T. Harada, Y. Kuniyoshi, and D. Cremers.
 1087 Elastic net constraints for shape matching. In *Proceedings of the IEEE International Conference on Computer*
 1088 *Vision*, pages 1169–1176, 2013. 2
- 1089 [20] R. B. Rusu, N. Blodow, and M. Beetz. Fast point feature
 1090 histograms (fpfh) for 3d registration. In *Robotics and Auto-*
 1091 *mation, 2009. ICRA'09. IEEE International Conference on*, pages 3212–3217. Citeseer, 2009. 1, 2
- 1092 [21] R. B. Rusu, Z. C. Marton, N. Blodow, and M. Beetz. Learning
 1093 informative point classes for the acquisition of object
 1094 model maps. In *Control, Automation, Robotics and Vi-*
 1095 *sion, 2008. ICARCV 2008. 10th International Conference on*, pages 643–650. IEEE, 2008. 2
- 1096 [22] R. B. Rusu, Z. C. Marton, N. Blodow, M. Dolha, and
 1097 M. Beetz. Towards 3d point cloud based object maps for
 1098 household environments. *Robotics and Autonomous Sys-*
 1099 *tems*, 56(11):927–941, 2008. 2
- 1100 [23] Y. Sahillioğlu and Y. Yemez. Scale normalization for iso-
 1101 metric shape matching. In *Computer Graphics Forum*, vol-
 1102 ume 31, pages 2233–2240. Wiley Online Library, 2012. 2
- 1103 [24] Y. Sahillioğlu and Y. Yemez. Multiple shape correspond-
 1104 ence by dynamic programming. In *Computer Graphics Forum*,
 1105 volume 33, pages 121–130. Wiley Online Library, 2014. 2
- 1106 [25] J. Solomon, G. Peyré, V. G. Kim, and S. Sra. Entropic metric
 1107 alignment for correspondence problems. *ACM Transac-*
 1108 *tions on Graphics (TOG)*, 35(4):72, 2016. 2
- 1109 [26] I. Talmi, R. Mechrez, and L. Zelnik-Manor. Template match-
 1110 ing with deformable diversity similarity. In *Proc. of IEEE*
 1111 *Conf. on Computer Vision and Pattern Recognition*, pages
 1311–1319, 2017. 1, 3
- 1112 [27] F. Tombari, S. Salti, and L. Di Stefano. Unique signatures of
 1113 histograms for local surface description. In *European con-*
 1114 *ference on computer vision*, pages 356–369. Springer, 2010.
 1115 2
- 1116 [28] A. Torsello. A game-theoretic approach to deformable shape
 1117 matching. In *Proceedings of the 2012 IEEE Conference on*
 1118 *Computer Vision and Pattern Recognition (CVPR), CVPR*
 1119 ‘12, pages 182–189, Washington, DC, USA, 2012. IEEE
 1120 Computer Society. 1, 2
- 1121 [29] M. Vestner, Z. Lähner, A. Boyarski, O. Litany, R. Slossberg,
 1122 T. Remez, E. Rodolà, A. Bronstein, M. Bronstein, R. Kimmel,
 1123 et al. Efficient deformable shape correspondence via
 1124 kernel matching. In *3D Vision (3DV), 2017 International*
 1125 *Conference on*, pages 517–526. IEEE, 2017. 1, 2
- 1126 [30] M. Vestner, R. Litman, E. Rodolà, A. M. Bronstein, and
 1127 D. Cremers. Product manifold filter: Non-rigid shape corre-
 1128 spondence via kernel density estimation in the product space.
 1129 In *CVPR*, pages 6681–6690, 2017. 2

References

- 1130 [1] D. Aiger, N. J. Mitra, and D. Cohen-Or. 4pointss congruent
 1131 sets for robust pairwise surface registration. *ACM Trans-*
 1132 *Graph.*, 27(3):85:1–85:10, Aug. 2008. 2
- 1133 [2] N. Aigerman, R. Poranne, and Y. Lipman. Seamless surface
 1134 mappings. *ACM Transactions on Graphics (TOG)*, 34(4):72,
 1135 2015. 2
- 1136 [3] M. Aubry, U. Schlickewei, and D. Cremers. The wave kernel
 1137 signature: A quantum mechanical approach to shape analy-
 1138 sis. In *Computer Vision Workshops (ICCV Workshops), 2011*
 1139 *IEEE International Conference on*, pages 1626–1633. IEEE,
 1140 2011. 2
- 1141 [4] A. M. Bronstein and M. M. Bronstein. Not only size mat-
 1142 ters: regularized partial matching of nonrigid shapes. In
 1143 *Computer Vision and Pattern Recognition Workshops, 2008.*
 1144 *CVPRW'08. IEEE Computer Society Conference on*, pages
 1145 1–6. IEEE, 2008. 1, 2
- 1146 [5] A. M. Bronstein, M. M. Bronstein, A. M. Bruckstein, and
 1147 R. Kimmel. Partial similarity of objects, or how to compare a
 1148 centaur to a horse. *International Journal of Computer Vision*,
 1149 84(2):163, 2009. 2
- 1150 [6] A. M. Bronstein, M. M. Bronstein, and R. Kimmel. Gener-
 1151 alized multidimensional scaling: a framework for isometry-
 1152 invariant partial surface matching. *Proceedings of the Na-*
 1153 *tional Academy of Sciences*, 103(5):1168–1172, 2006. 1
- 1154 [7] M. M. Bronstein and I. Kokkinos. Scale-invariant heat ker-
 1155 nel signatures for non-rigid shape recognition. In *Computer*
 1156 *Vision and Pattern Recognition (CVPR), 2010 IEEE Confer-*
 1157 *ence on*, pages 1704–1711. IEEE, 2010. 2
- 1158 [8] L. Cosmo, E. Rodolà, M. Bronstein, A. Torsello, D. Cremers,
 1159 and Y. Sahillioglu. Shrec’16: Partial matching of deformable
 1160 shapes. *Proc. 3DOR*, 2, 2016. 1, 7
- 1161 [9] T. Dekel, S. Oron, M. Rubinstein, S. Avidan, and W. T. Free-
 1162 man. Best-buddies similarity for robust template matching.
 1163 In *Proceedings of the IEEE Conference on Computer Vision*
 1164 *and Pattern Recognition*, pages 2021–2029, 2015. 3
- 1165 [10] D. Holz, A. E. Ichim, F. Tombari, R. B. Rusu, and S. Behnke.
 1166 Registration with the point cloud library: A modular frame-
 1167 work for aligning in 3-d. *IEEE Robotics & Automation Mag-*
 1168 *azine*, 22(4):110–124, 2015. 1
- 1169 [11] V. G. Kim, Y. Lipman, and T. Funkhouser. Blended intrinsic
 1170 maps. In *ACM Transactions on Graphics (TOG)*, volume 30,
 1171 page 79. ACM, 2011. 7
- 1172 [12] A. Kovnatsky, M. M. Bronstein, X. Bresson, and P. Van-
 1173 derghenrst. Functional correspondence by matrix comple-
 1174 tion. In *Proceedings of the IEEE conference on computer*
 1175 *vision and pattern recognition*, pages 905–914, 2015. 2
- 1176 [13] O. Litany, E. Rodolà, A. M. Bronstein, and M. M. Bronstein.
 1177 Fully spectral partial shape matching. In *Computer Graphics*
 1178 *Forum*, volume 36, pages 247–258. Wiley Online Library,
 1179 2017. 1, 2, 8
- 1180 [14] H. Maron, N. Dym, I. Kezurer, S. Kovalsky, and Y. Lip-
 1181 man. Point registration via efficient convex relaxation. *ACM*
 1182 *Transactions on Graphics (TOG)*, 35(4):73, 2016. 2
- 1183 [15] M. Ovsjanikov, M. Ben-Chen, J. Solomon, A. Butscher, and
 1184 L. Guibas. Functional maps: A flexible representation of
 1185 1186 1187

- 1188 maps between shapes. *ACM Trans. Graph.*, 31(4):30:1–
1189 30:11, July 2012. 1, 2 1242
1190 [16] J. Pokrass, A. M. Bronstein, and M. M. Bronstein. Partial 1243
1191 shape matching without point-wise correspondence. *Numerical 1244
1192 Mathematics: Theory, Methods and Applications*, 6(1):223–244, 1245
1193 2013. 2 1246
1194 [17] J. Pokrass, A. M. Bronstein, M. M. Bronstein, P. Sprech- 1247
1195 mann, and G. Sapiro. Sparse modeling of intrinsic cor- 1248
1196 respondences. In *Computer Graphics Forum*, volume 32, 1249
1197 pages 459–468. Wiley Online Library, 2013. 2 1250
1198 [18] E. Rodolà, L. Cosmo, M. M. Bronstein, A. Torsello, and 1251
1199 D. Cremers. Partial functional correspondence. In *Computer 1252
1200 Graphics Forum*, volume 36, pages 222–236. Wiley Online 1253
1201 Library, 2017. 1, 2 1254
1202 [19] E. Rodolà, A. Torsello, T. Harada, Y. Kuniyoshi, and D. Cre- 1255
1203 mers. Elastic net constraints for shape matching. In *Pro- 1256
1204 ceedings of the IEEE International Conference on Computer 1257
1205 Vision*, pages 1169–1176, 2013. 2 1258
1206 [20] R. B. Rusu, N. Blodow, and M. Beetz. Fast point feature 1259
1207 histograms (fpfh) for 3d registration. In *Robotics and Au- 1260
1208 tonation, 2009. ICRA’09. IEEE International Conference 1261
1209 on*, pages 3212–3217. Citeseer, 2009. 1, 2 1262
1210 [21] R. B. Rusu, Z. C. Marton, N. Blodow, and M. Beetz. Learn- 1263
1211 ing informative point classes for the acquisition of object 1264
1212 model maps. In *Control, Automation, Robotics and Vi- 1265
1213 sion, 2008. ICARCV 2008. 10th International Conference 1266
1214 on*, pages 643–650. IEEE, 2008. 2 1267
1215 [22] R. B. Rusu, Z. C. Marton, N. Blodow, M. Dolha, and 1268
1216 M. Beetz. Towards 3d point cloud based object maps for 1269
1217 household environments. *Robotics and Autonomous Sys- 1270
1218 tems*, 56(11):927–941, 2008. 2 1271
1219 [23] Y. Sahillioğlu and Y. Yemez. Scale normalization for iso- 1272
1220 metric shape matching. In *Computer Graphics Forum*, vol- 1273
1221 ume 31, pages 2233–2240. Wiley Online Library, 2012. 2 1274
1222 [24] Y. Sahillioğlu and Y. Yemez. Multiple shape correspond- 1275
1223 ence by dynamic programming. In *Computer Graphics Forum*, 1276
1224 volume 33, pages 121–130. Wiley Online Library, 2014. 2 1277
1225 [25] J. Solomon, G. Peyré, V. G. Kim, and S. Sra. Entropic metric 1278
1226 alignment for correspondence problems. *ACM Transactions 1279
1227 on Graphics (TOG)*, 35(4):72, 2016. 2 1280
1228 [26] I. Talmi, R. Mechrez, and L. Zelnik-Manor. Template 1281
1229 matching with deformable diversity similarity. In *Proc. of IEEE 1282
1230 Conf. on Computer Vision and Pattern Recognition*, pages 1283
1231 1311–1319, 2017. 1, 3 1284
1232 [27] F. Tombari, S. Salti, and L. Di Stefano. Unique signatures 1285
1233 of histograms for local surface description. In *European 1286
1234 conference on computer vision*, pages 356–369. Springer, 2010. 1287
1235 2 1288
1236 [28] A. Torsello. A game-theoretic approach to deformable shape 1289
1237 matching. In *Proceedings of the 2012 IEEE Conference on 1290
1238 Computer Vision and Pattern Recognition (CVPR), CVPR 1291
1239 ’12*, pages 182–189, Washington, DC, USA, 2012. IEEE 1292
1240 Computer Society. 1, 2 1293
1241 [29] M. Vestner, Z. Lähner, A. Boyarski, O. Litany, R. Slossberg, 1294
1242 T. Remez, E. Rodolà, A. Bronstein, M. Bronstein, R. Kim- 1295
1243 mel, et al. Efficient deformable shape correspondence via 1296
1244 kernel matching. In *3D Vision (3DV), 2017 International 1297
1245 Conference on*, pages 517–526. IEEE, 2017. 1, 2 1298

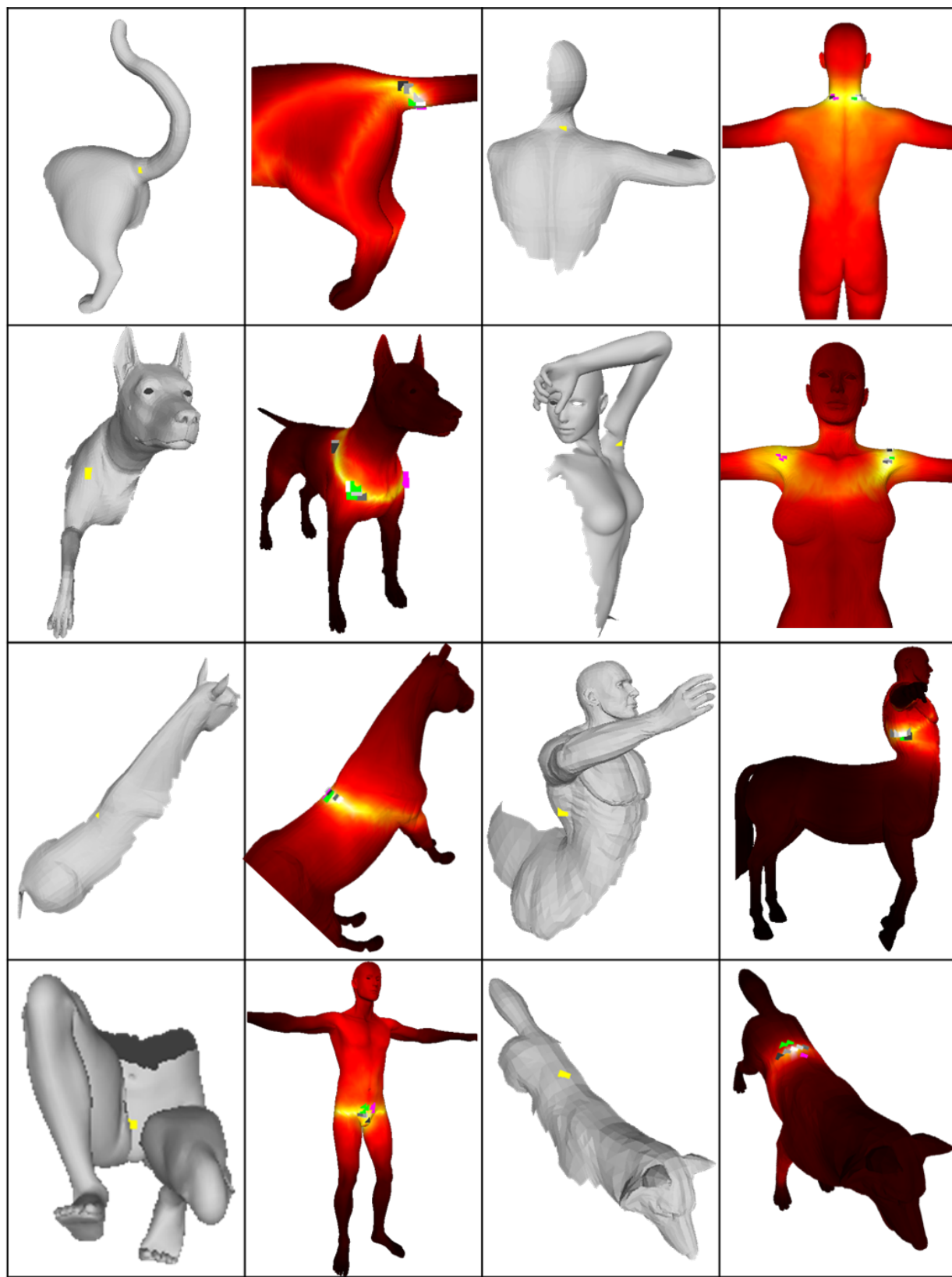
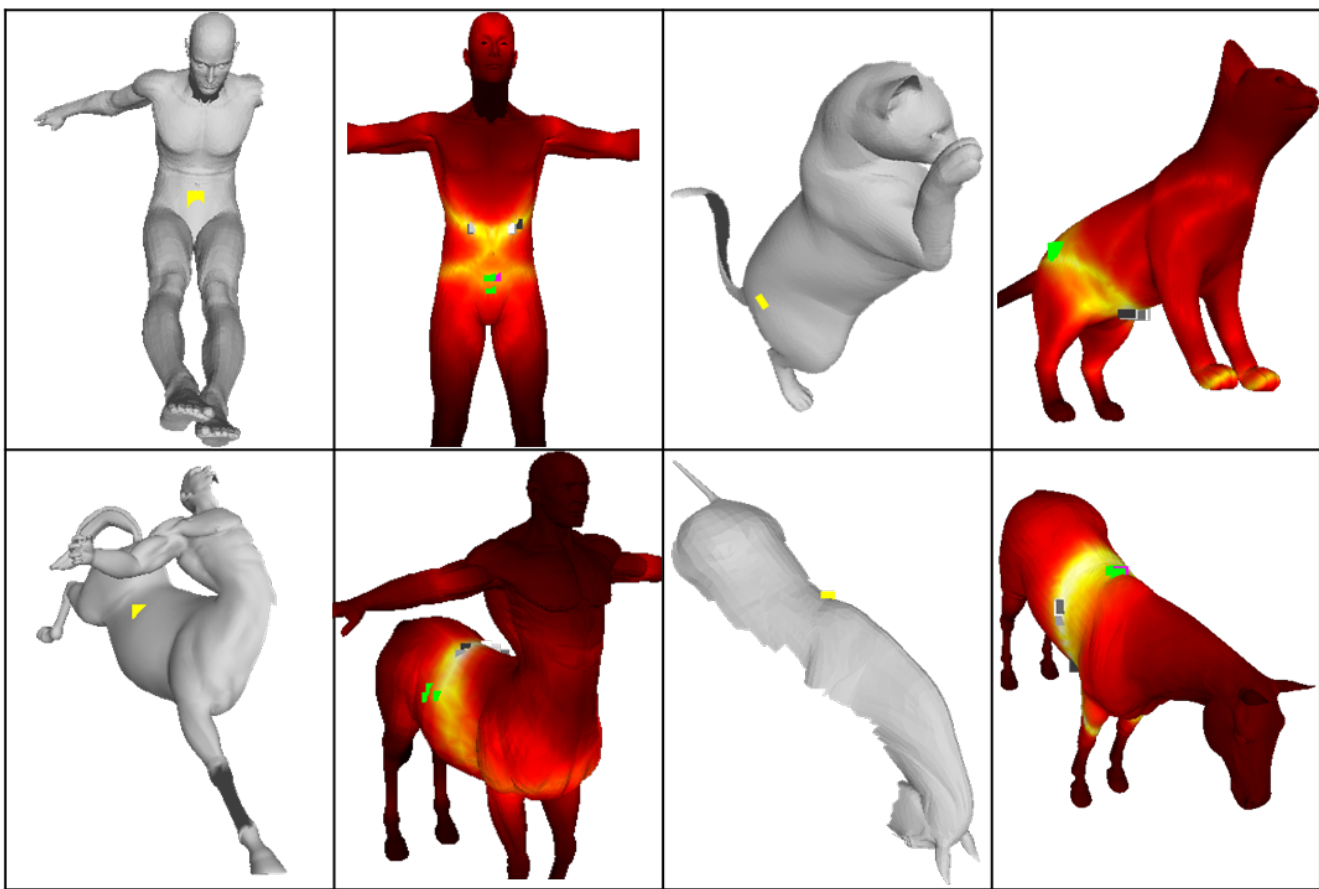
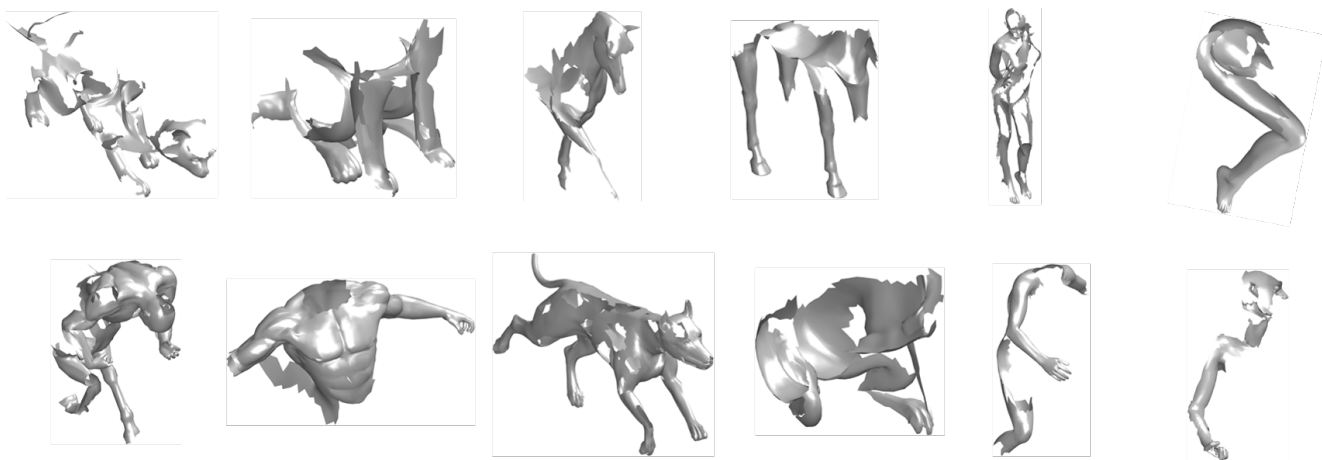


Figure 10. Some examples of cuts and their matching similarity score maps. The compared point is marked in yellow on the cut, whereas ground truth polygon is marked in green, symmetrical polygon in purple, and top 5 matches in grayscale

1296
1297
1298
1299
1300
1301
1302
1303
1304
1305
1306
1307
1308
1309
1310
1311
1312
1313
1314
1315
1316
1317
1318
1319
1320
1321
1322
1323
1324
1325
1326
1327
1328
1329
1330
1331
1332
1333
1334
1335
1336
1337
1338
1339
1340
1341
1342
1343
1344
1345
1346
1347
1348
1349
1350
1351
1352
1353
1354
1355
1356
1357
1358
1359
1360
1361
1362
1363
1364
1365
1366
1367
1368
1369
1370
1371
1372
1373
1374
1375
1376
1377
1378
1379
1380
1381
1382
1383
1384
1385
1386
1387
1388
1389
1390
1391
1392
1393
1394
1395
1396
1397
1398
1399
1400
1401
1402
1403

1404
1405
1406
1407
1408
1409
1410
1411
1412
1413
1414
1415
1416
1417
1418
1419
14201421
1422
1423
1424
1425
1426
1427
1428
1429
1430
1431
1432
1433
1434
1435
1436
1437
1438
1439
1440
1441
1442
1443
1444
1445
1446
1447
1448
1449
1450
1451
1452
1453
1454
1455
1456
1457
1458
1459
1460
1461
1462
1463
1464
1465
1466
1467
1468
1469
1470
1471
1472
1473
1474
1475
1476
1477
1478
1479
1480
1481
1482
1483
1484
1485
1486
1487
1488
1489
1490
1491
1492
1493
1494
1495
1496
1497
1498
1499
1500
1501
1502
1503
1504
1505
1506
1507
1508
1509
1510
15111458
1459
1460
1461
1462
1463
1464
1465
1466
1467
1468
1469
1470
1471
1472
1473
1474
1475
1476
1477
1478
1479
1480
1481
1482
1483
1484
1485
1486
1487
1488
1489
1490
1491
1492
1493
1494
1495
1496
1497
1498
1499
1500
1501
1502
1503
1504
1505
1506
1507
1508
1509
1510
1511

10

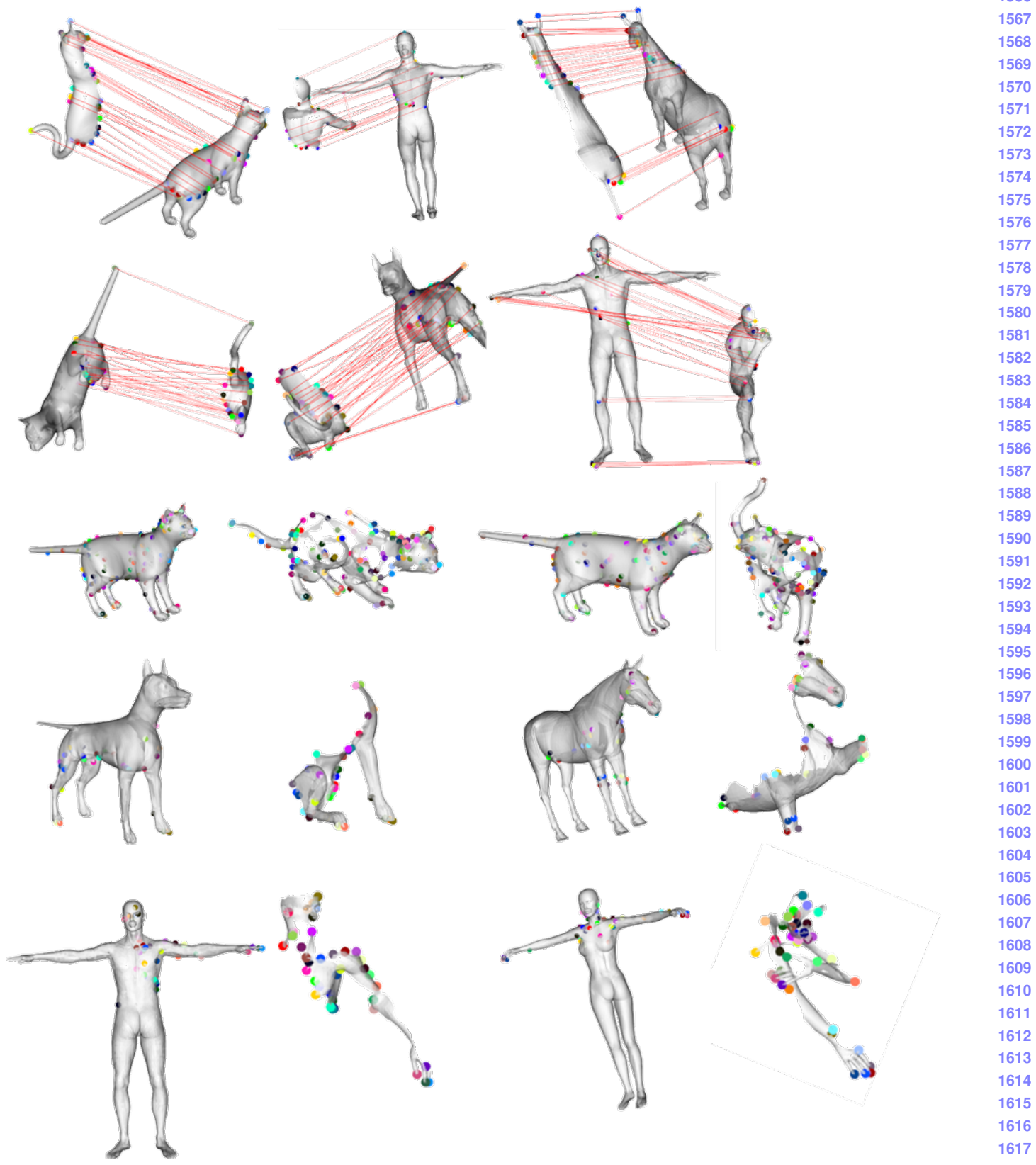


Figure 13. Good correspondences obtained by our DDIS measure

1620
1621
1622
1623
1624
1625
1626
1627
1628
1629
1630
1631
1632
1633
1634
1635
1636
1637
1638
1639
1640
1641
1642
1643
1644
1645
1646
1647
1648
1649
1650
1651
1652
1653
1654
1655
1656
1657
1658
1659
1660
1661
1662
1663
1664
1665
1666
1667
1668
1669
1670
1671
1672
1673

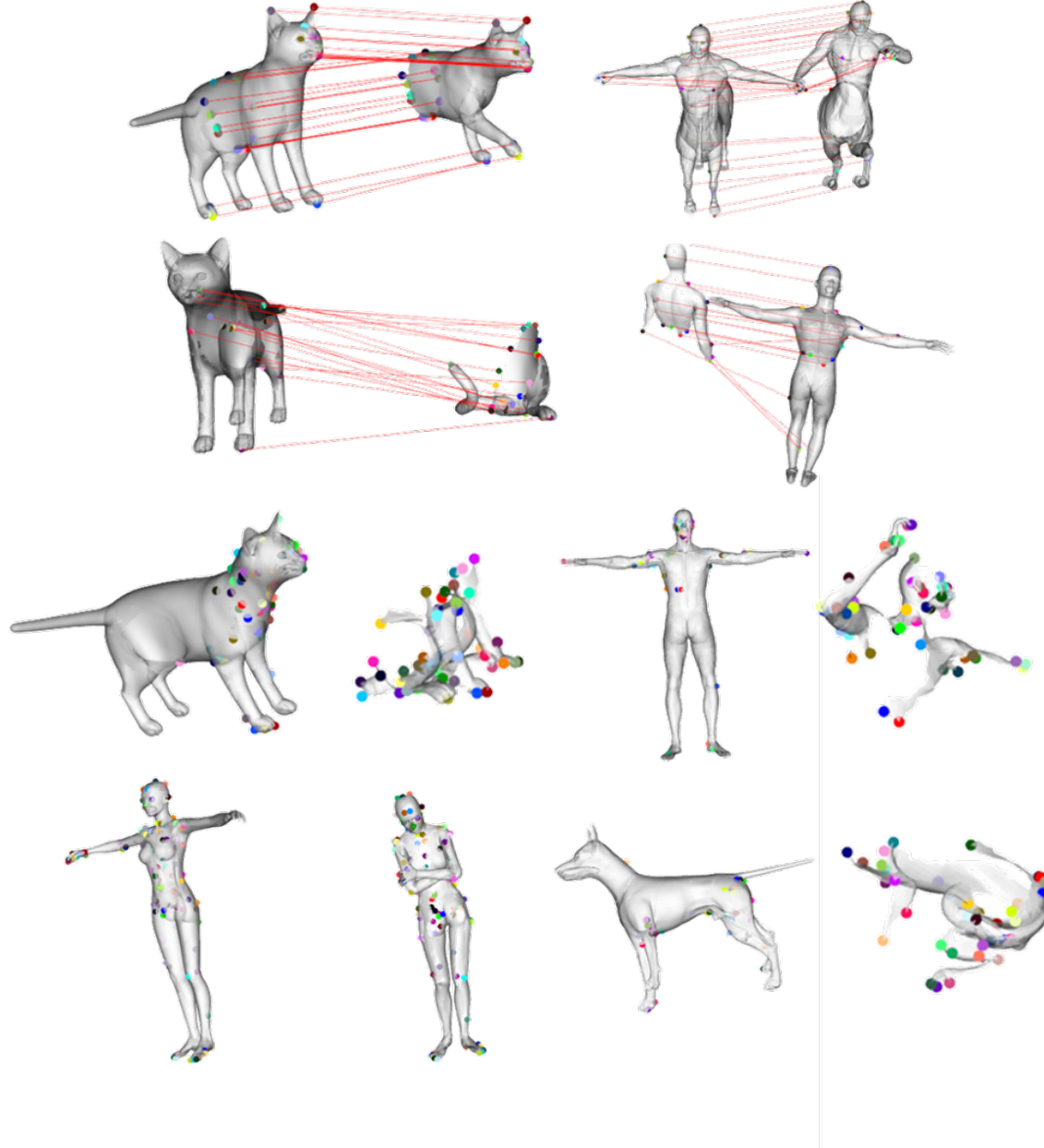


Figure 14. Some notable failure cases - most common is cat paw assignment - an extrinsic near symmetry gives rise to this phenomena. Closed fists on humanoids tends to cause a collapse of all fingers to a single finger. In the holes extreme partiality makes the geodesic distances break even over short distances.

1674
1675
1676
1677
1678
1679
1680
1681
1682
1683
1684
1685
1686
1687
1688
1689
1690
1691
1692
1693
1694
1695
1696
1697
1698
1699
1700
1701
1702
1703
1704
1705
1706
1707
1708
1709
1710
1711
1712
1713
1714
1715
1716
1717
1718
1719
1720
1721
1722
1723
1724
1725
1726
1727